Controlling Ultracold molecules

This report recaps molecules in external fields and their use in Ramsey interferometry for precision measurements. A limit on the Rabi frequency of pulses for the 2-level approximation to be valid is found. The method of applying pulses to extend coherence time is tested for a range of background noise. A theory for finding optimal pulse timings for decoupling is combined with the pulse sequences and ways of finding optimal pulse timings for noise that is well known or can be approximated is shown. The effect of changing the pulse timing for the same pulse sequence was shown to give an improvement on the coherence time by a factor of ≈ 4.7 which in an experiment would require no additional power use. A method of combining pulses and making general pulse sequences more robust is given and tested for the well know XY4 pulse. Future methods for robust pulses to test for making further improvements for coherence are mentioned.

CONTENTS

1. INTRODUCTION

The ultracold regime is temperatures below a mk. Ultracold atoms and molecules have many uses such as, but not limited to, cold controlled chemistry, quantum computing, precision measurement for testing models and quantum simulations [1,2,3,4,5,6,7]. Some exciting possible uses of ultracold atoms or molecules could be Shor's quantum computer algorithm [10] and adiabatic computation [11] both show how quantum algorithms can scale much more effectively to manage complex calculations that would take years of classical computing power, demonstrating how useful the technology can be. For any of these applications the effects between the system and environment need to be minimised to reduce decoherence to allow for longer and more complicated experiments involving quantum information. In this report the method focused on for removing the system-environment coupling is pulse sequences. Using a pulse to reduce decoherence was introduced in 1950 [28] in the context of Nuclear Magnetic Resonance (NMR) to reverse the effect of dephasing. This method was extended by applying additional pulses in the time interval of the experiment but was not used in the context of quantum information processing until the 1990s [29]. Since then more work has been done and these techniques have been developed to reduce the effects of general, unknown noise [30, 31]. The long lifetime of the rotational states can be calculated using [40]:

$$\Gamma = \frac{\omega_0^3}{3\pi\epsilon_0\hbar c^3}|\langle e|\vec{d}|g\rangle|^2, \omega \approx 1000GHz, \vec{d} \approx 1\text{debeye} \tag{1}$$

to be approximately 4000 years. For ultracold molecules, this means that the main problem for coherence in the time frame of experiments are dephasing effects (see decoherence section).The first challenge of using ultracold molecules is cooling and preparing a sample to one specific state, usually the ground state. For singular atoms there are many techniques with in-depth research [8]. However for ultracold molecules the process is more complex and these techniques used for atoms need to be adapted for forming molecules due to the much larger set of internal states[9]: this will be discussed further later.

Polar molecules are very versatile in their applications due to their rich internal structure coming from their many hyperfine states. For example, this report focuses on RbCs which has 32 - $(2I_{Rb}+1)(2I_{Cs}+1)$ hyperfine states in the rotational ground state while as atoms, Rb and Cs would only have 4 - $(2I_{Rb}+1)$ and 8 - $(2I_{Cs}+1)$ hyperfine states. Their ability to rotate and vibrate compared to atoms gives more freedom to create and find energy level structures for a desired use. Polar molecules have large permanent dipoles that can be used for long range dipole-dipole interactions (DDI) can be induced. These DDI are can be used and controlled and act further than just the neighbouring molecules to study many-body systems and more advanced quantum simulations [12]. They are also anisotropic. Very large internal fields can be made to simulate extreme conditions for the molecules bound electrons in experiments that can test the standard model by measuring the electrons electric dipole moment[28]. RbCs in its absolute ground state has been shown to be stable in the exchange reactions: (fig), molecules with one of these reactions exothermic can have faster loss rates that would give stricter lifetimes for experiments [13].However the molecules can still be lost when they collide and form a '2-body complex' which can be excited by the optical trap causing them to be removed from the experiment [27].

2. GROUND STATE PREPARATION

A given rotationally excited state may decay back into multiple different ground states so cooling molecules to ultracold temperatures is much more complex than atoms since laser cooling relies on cycling between a set of states. A more in depth discussion of these transitions is discussed later. To get around this problem, usually the two atom types of the molecule are cooled to a desired temperature and then used to form molecules.

A. How to get ultracold temperatures

Laser cooling can be used to get atoms down to μk by colliding the atoms with photons that slows the atom down in the absorbed direction. Later the same frequency photon is emitted in a random direction so that over time this method can be repeated for 1000s of cycles as long as the transition is closed so the atom cycles between two specific states. Overtime the overall momentum change due to the emitted photons is zero since the direction is random. The momentum is decreased from absorbing incoming photons. Finding closed transitions is much harder for molecules due to having much more different spin states. Due to this, this method is usually not used directly on them.

B. How to form molecules

One of the main methods used to form molecules is by using Feshbach resonances in magnetoassociation. This method to form molecules is done by varying the magnetic field near a Feshbach resonance molecules can be made. At ultracold temperatures the collision of two atoms is described by the scattering length. If the atoms or the molecule or both are paramagnetic, the potential of the collision can be manipulated by an external magnetic field. By starting the magnetic field above the resonant point and lowering it slow enough the atoms follow the avoided crossing of the unbound and bound state energies being equal and can finish in the molecular state.

C. Transferring to the ground state

Once formed, the molecules can be put into the ground state by Stimulated Raman Adiabatic Passage (STIRAP). This method works for two states that aren't directly connected by coupling the initial and final state to an intermediate state which is never populated during the transfer. This method has been able to achieve 100 percent efficiency in other applications and was show to work in experiments under light intensity variations.[14,15]

3. HAMILTONIAN OF A DIATOMIC MOLECULE

For a molecule at ultracold temperatures, the motion is negligible due to the temperature and optical trap, the vibrational state is fixed so the total Hamiltonian can be wrote as:

$$H_{\rm tot} = H_{\rm rot} + H_{\rm hf} + H_{\rm ext}, \tag{2}$$

with $H_{\rm rot}$ describing the rotational structure, $H_{\rm hf}$ describing any hyperfine interactions and $H_{\rm ext}$ describing the molecule in any external fields applied.

A. Rotational

For diatomic molecules, $H_{\rm rot}$ can be described by using a rigid rotor model and results in energy levels of approximately $E_N \approx B_v N(N+1)$ where N is the rotational level[26]. B_v is the rotational constant of the molecule in the vibrational state v. So the overall contribution to a molecules rotational structure is:

$$H_{rot} = B_v(\boldsymbol{N}\cdot\boldsymbol{N}) - D_v(\boldsymbol{N}\cdot\boldsymbol{N})^2 \tag{3}$$

when including a distortion term with distortion coefficient equal to D_v.

B. Hyperfine

The hyperfine Hamiltonian covers interactions between the nuclear spins and their interactions with the molecule's angular momenta[16]. This Hamiltonian can be separated as:

$$H_{\rm hf} = H_{\rm quad} + H^{(0)}_{\rm spin-spin} + H^{(2)}_{\rm spin-spin} + H_{\rm spin-rotation} \tag{4}$$

$H_{\rm quad}$ is from the electric quadrupole due to the charge being non-uniform around the two atoms and can be represented by:

$$H_{\rm quad} = \sum_{i=A,B} e\mathbf{Q}_i \cdot \mathbf{q}_i, \tag{5}$$

$e\mathbf{Q}_i$, $\mathbf{q}_i$ are the nuclear quadrupole moment and the electric field gradient at nucleus i. This term is only non-zero for nuclear terms that have spin greater than 1/2.

$H^{(0)}_{spin-spin}$ and $H^{(2)}_{spin-spin}$ describe the scalar and tensor interactions of the nuclear spins:

$$H^{(0)}_{\rm spin-spin} = c_4 \boldsymbol{I}_A \cdot \boldsymbol{I}_B \tag{6}$$

$$H^{(2)}_{\rm spin-spin} = -c_3\sqrt{6}\mathbf{T}^2(\boldsymbol{C})\cdot\mathbf{T}^2(\boldsymbol{I}_A,\boldsymbol{I}_B) \tag{7}$$

These terms depend on the molecule's constants $c_{3,4}$ and the rank 2 tensors. The angles of $T^2_q(C) = C^2_q(\theta,\phi)$ are the polar angle θ, and the azimuthal angle ϕ of the molecules axis from z which, in the code used later, is defined by the direction of the applied external fields. $\mathbf{T}^2(\boldsymbol{I}_A,\boldsymbol{I}_B)$ is a rank 2 tensor product of the nuclear spins.

$H_{spin-rotation}$ describes how the nuclear spins interact with the magnetic field caused by the rotating molecule as is given by:

$$H_{\mathrm{spin-rotation}} = \sum_{i=A,B} c_i \boldsymbol{N} \cdot \boldsymbol{I_i} \tag{8}$$

C. External fields

The hamiltonian components from external fields in the experimental setup can be separated into: $H_{\mathrm{ext}} = H_z + H_{dc} + H_{ac}$, which come from DC magnetic fields, DC electric fields and AC electric fields.

$$H_{\mathrm{z}} = -g_r \mu_N \boldsymbol{N} \cdot \boldsymbol{B} - \sum_{i=A,B} g_i (1-\sigma_i) \mu_N \boldsymbol{I}_i \cdot \boldsymbol{B} \tag{9}$$

includes how the molecules rotation and the nuclear spins interact with the magnetic field applied. DC electric fields can be used to align the molecules since polar molecules have permanent dipoles.

$$H_{\mathrm{dc}} = -\mu_0 \boldsymbol{E}_{dc} \cdot \hat{n} \tag{10}$$

These fields cause energy levels with different Mn values to be split which is more clearly seen by looking at the matrix elements of the dipole operator. [17]

Most ultracold experiments involve optical traps which are formed from oscillating fields. The molecules will mainly interact with the traps electric field since the magnetic field component is much smaller. For an optical field with electric field E_{ac}, it gives a hamiltonian:

$$H_{\mathrm{ac}} = -\frac{1}{2} \boldsymbol{E}_{ac} \cdot \alpha \cdot \boldsymbol{E}_{ac} \tag{11}$$

where the laser intensity, $I_{ac} = E_{ac}^2/(\epsilon_0 c)$. Alpha is the molecules polarisabilty tensor which depends on the light wavelength used. The polarisabilty is not equal for all directions of fields applied, for a molecule at an angle θ to the laser's polarisation, the polarisibilty is: $\alpha(\theta) = \alpha_{\parallel}$ $\cos^2(\theta)$ + $\alpha_{\perp}$ $\sin^2(\theta)$ = $\alpha^{(0)} + \alpha^{(2)} P_2(\cos\theta)$

4. DIATOMIC PYTHON MODULE

Using the diatomic module, [16] the Separate Hamiltonian terms in an uncoupled basis can be formed.For the code to work for a given molecule species, it's constants are either imported from the module or manually inputted as a python dictionary. The external field components are formed independent of field magnitudes and then can be multiplied by array of field magnitude values to model changing fields. These external fields define the $\vec{z}$ axis. The two nuclei are labelled A and B and then the quantum numbers used are N, I_A, I_B for the molecules rotational and nuclear spin angular momenta. Along with their projections onto the applied external fields, M_n, M_A, M_B, the basis states can be wrote as $|N, MN, m_A, m_B\rangle$. The angular momenta are created using ladder operators. [16]

5. RBCS IN EXTERNAL FIELDS

Controlling any experimental system in physics is key to retrieving accurate and precise results. A solid understanding of how molecules interact with external fields from the experimental setup is needed and can be used to find values of fields where random fluctuations are minimised or well understood.

A. Zeeman effect

A magnetic field can be used to split energy levels depending on the nuclear spins.

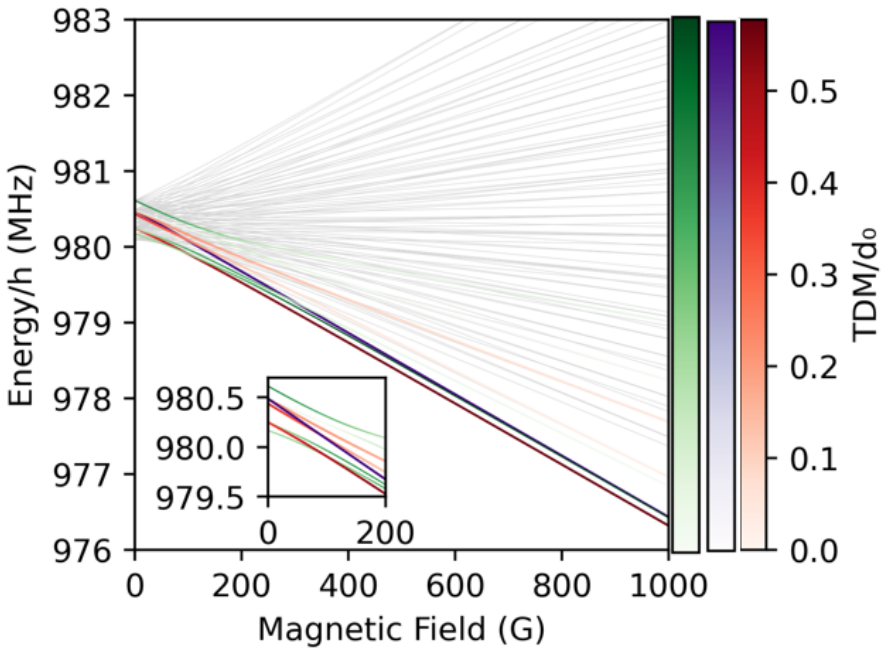

FIG. 1: Energy structure of the first rotational level in a varying magnetic field. States are colour coded based on Mn value.Purple,red,green corresponds to Mf = +1,0,-1. When the hyperfine mixing is prevalent, the different spin states cause the zeeman shift to be non linear.

Due to the hyperfine interactions, the eigenstates have mixed compositions made up from the different basis functions with different Mn and nuclear spin components but equal overall Mf values. This mixing is more prevalent at smaller magnetic field values up until the Zeeman perturbation is of a larger magnitude to the hyperfine interactions and dominates the molecules hamiltonian. The main consequence of this state mixing is that additional transitions can be observed . Since the wave functions of the different hyperfine states mix, the Zeeman shift of magnetic sublevels is non-linear with an increasing magnetic field. At low fields, the molecules total angular momentum is $F = N + I_{Rb} + I_{Cs}$ and so transitions $\Delta F = 0, \pm 1$ and $\Delta M_F = 0, \pm 1$ can be found by a change in momentum depending on the photons polarisation. However, at higher fields the nuclear spins decouple so new quantum numbers are needed to be used and only Mn changes in transitions, so at most only 3 transitions can occur.

From table1 in the appendix, the different nuclear spin sums are shown to make the Mf values clearer.

As the field strength changes the value of the transition dipole moments (TDM) between these rotational sublevels and the ground state of the molecule change from their unperturbed values due to the state composition changing. For RbCs, only the N=1, Mf=6 state does not have a mixed composition, since the two nuclear spins are at their maximum there is no other way for Mf=6 to be made. This causes this state to be the only state that the TDM remains unchanged as the field magnitude changes and the Zeeman shift to be linearly proportional to the field. At low field, more transitions than expected by the selection rules can be observed due to all Mf levels containing an element of an allowed transitions of the dipole operator. For the limit of large magnetic field, the TDM values approach the expected case when hyperfine interactions are minimal/ignored due to the Zeeman splitting being the most dominant effect.

By looking at the limiting state composition, these 3 states contain the components with unchanged nuclear spin from the ground state and $M_N = 0, \pm 1$ so are allowed by the operator.

B. DC electric field

In a constant electric field, the different rotational states of the molecules are perturbed depending on their Mn values.

The strength of the DC field can be manipulated to reduce the complexity of the 'extra' observed transitions by causing a perturbation stronger than the hyperfine splitting that will erase the mixed state composition. Compared to a magnetic field, it takes a much smaller electric field to stop the additional transitions and at around 0.08kV/cm only 3 allowed transitions are prevalent. Unlike magnetic fields, the DC stark effect causes states to couple to higher rotational levels with the same nuclear spins and equal Mn values (to the state you're looking at).At very high field strengths, the other rotational levels dominate the state composition. The transition dipole moment between this state and the N=1 states also decrease with an increasing field due to the transitions from other rotational states being forbidden which can be seen by looking at the Wigner-3j symbol in the dipole operator.

In a Dc electric field, the hyperfine mixing is overcome at very low fields since the RbCs molecules have natural dipole moments so only the different rotational level components are relevant. As the field increases more rotational levels are significant in the state composition and these components effect the TDM values.

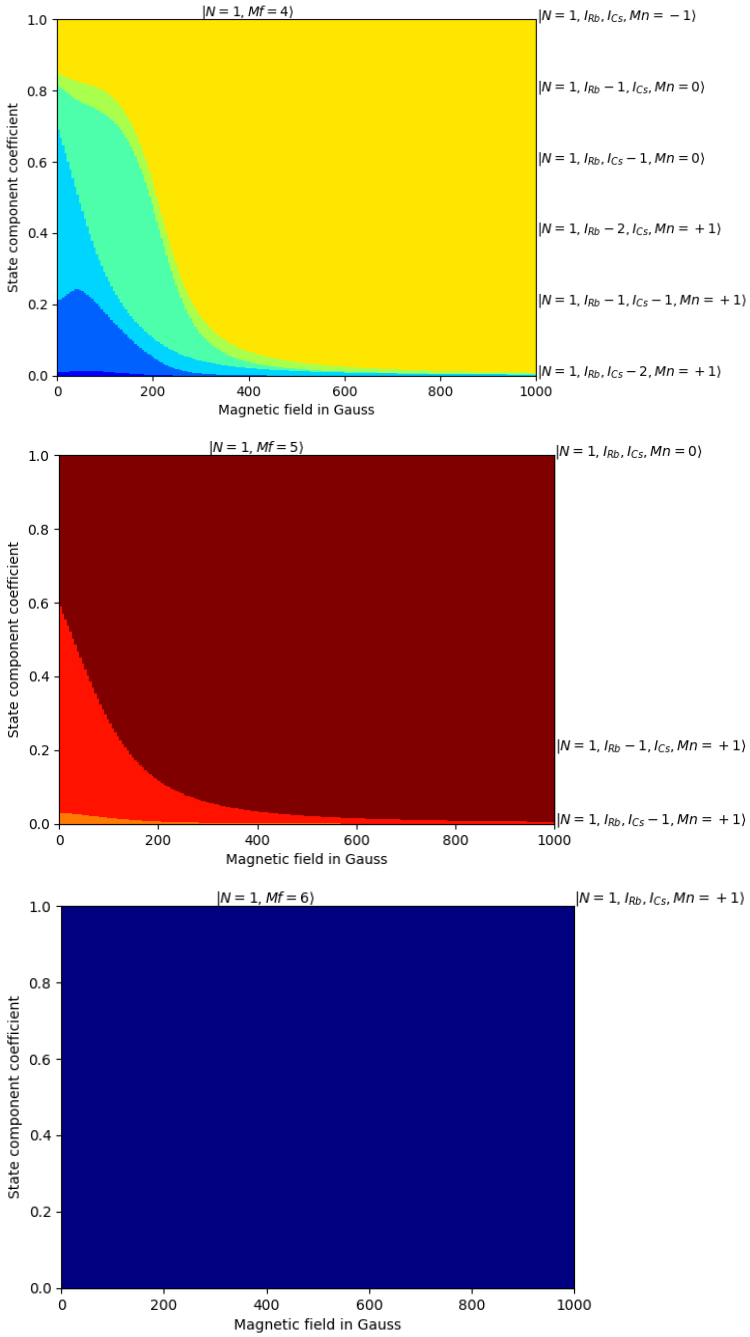

FIG. 2: Composition variation in magnetic field strength of the 3 transitions seen in a high magnetic field. All 3 states have a high field limit composition made up from only a state with unchanged nuclear spins.

C. AC stark

In an optical trap when the molecules axis is well defined by an external field, by varying the angle that the AC field is applied a different energy shift occurs at equal field intensity. From this, magic angles can be found in which the energy shift is minimised and equal to 0.
When the orientation of the molecules is well defined by an external DC electric field these magic angles can be exploited in experiments to trap the molecules without changing the tran-

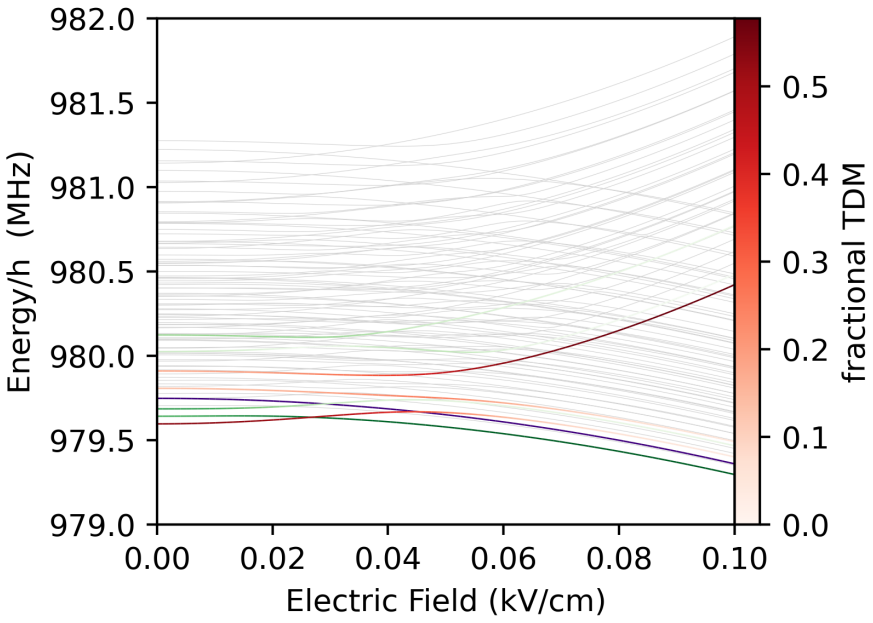

FIG. 3: Energy structure of the first rotational state in a DC electric field

sition energy between of any of the states therefore reducing any extra contribution to decoherence.An angle of 54.7 was used for the magic angle as this cancels the effects of the anisotropic polarisibilty tensor.

6. RABI OSCILLATIONS

Focusing on the first rotational state transitions, they have transition frequencies close to 1 GHz which is in the microwave range of the EM spectrum so changing the field frequency can be fine tuned. When a two-level system is radiated by resonant field

$$\vec{E} = E_0 cos(\omega t + \phi), \tag{12}$$

the population of the two states will oscillate sinusoidal at a rate inversely proportional to the transition dipole moment between the states. For a system driven by a monochromatic field of a frequency of w, the two states couple together through their dipole moment, $\vec{d}$. The interaction Hamiltonian is given by:

$$H = \frac{\hbar}{2}\begin{pmatrix} \Delta & \Omega e^{-i\phi} \\ \Omega e^{i\phi} & -\Delta \end{pmatrix}. \tag{13}$$

The hamiltonian component that describes how the system interacts with the radiation is then $\vec{V} = \vec{d} \cdot E$. By looking at the time evolution of the states and defining the Rabi frequency: $\Omega = \frac{E_0}{\hbar}\langle e|\vec{d} \cdot E|g\rangle$, the state will be back in it's initial population after $T = 2\pi/\Omega$. The inverse relation between time and the Rabi frequency is confirmed by varying the pulse time and tracking the final state population: see first appendix item. For detuned oscillations, the Rabi frequency is altered to $\Omega_{eff} = \sqrt{(\Omega^2 + \Delta^2)}$ and the oscillations become faster regardless of the detuning being negative or positive. Another key feature is that the amplitude of the

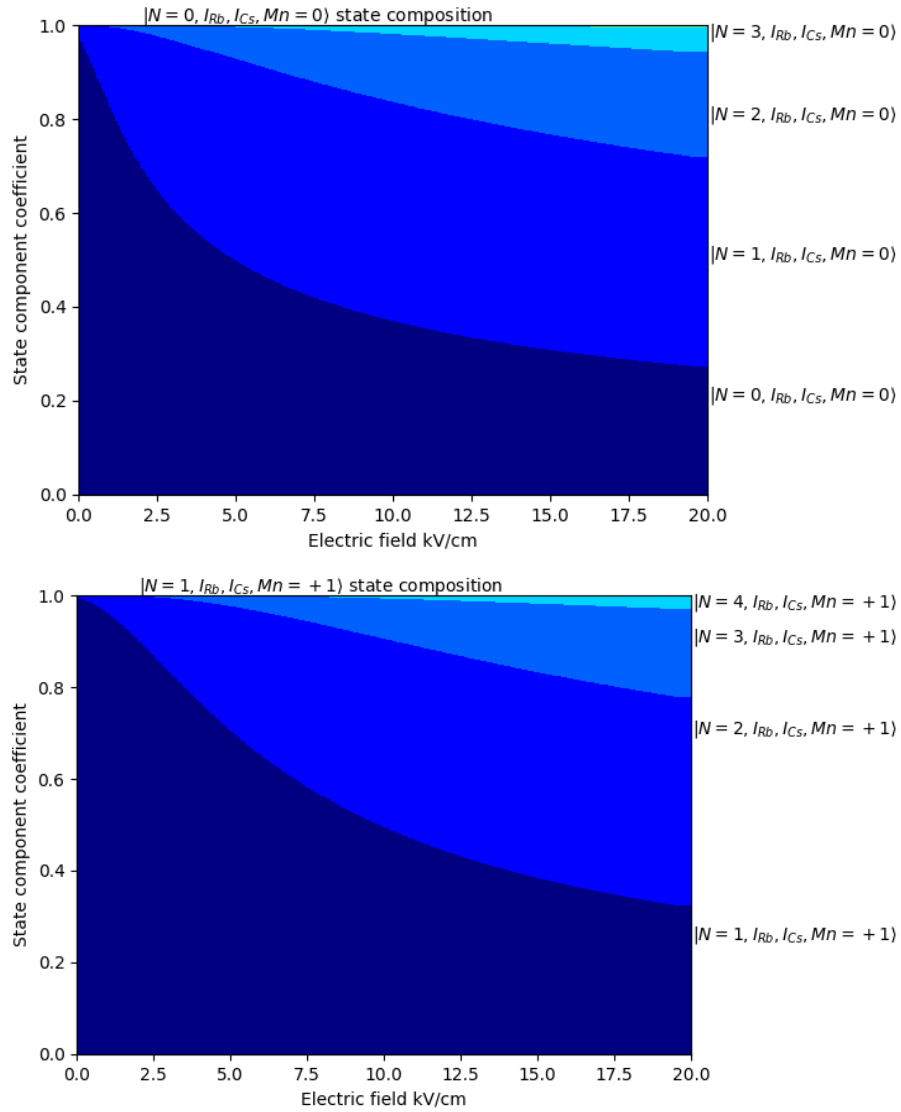

FIG. 4: State composition of the ground state and $M_f = 6$ excited state in changing electric field strength. Eigenstates now have a composition that mixes states with equal Mf and Mn values

oscillations become smaller and a proportion of the state is trapped in the ground state. On Figure 6, since the x-axis units are divided by the original Rabi frequency it shows how for a fixed detuning, increasing the Rabi frequency can lower the effect on the population transfer. Due to the long lifetime of the rotational states, the oscillations are coherent and the amplitude does not decay in the time frame for experiments to finish.When the field is resonant, applying a pulse of a time duration $T = \pi/\Omega$ is classed as a $\pi - pulse$. If the atom is initially in the ground state, then a $\pi-$pulse transfers it to the excited state: it completely flips the population. If the duration of the pulse is halved that $T = \pi/2\Omega$, then it is classed as a $\pi/2$-pulse. From being initially fully in one state (excited or ground) , this transfers the system into an equal superposition of both the ground and excited state. A general pulse can be represented by the

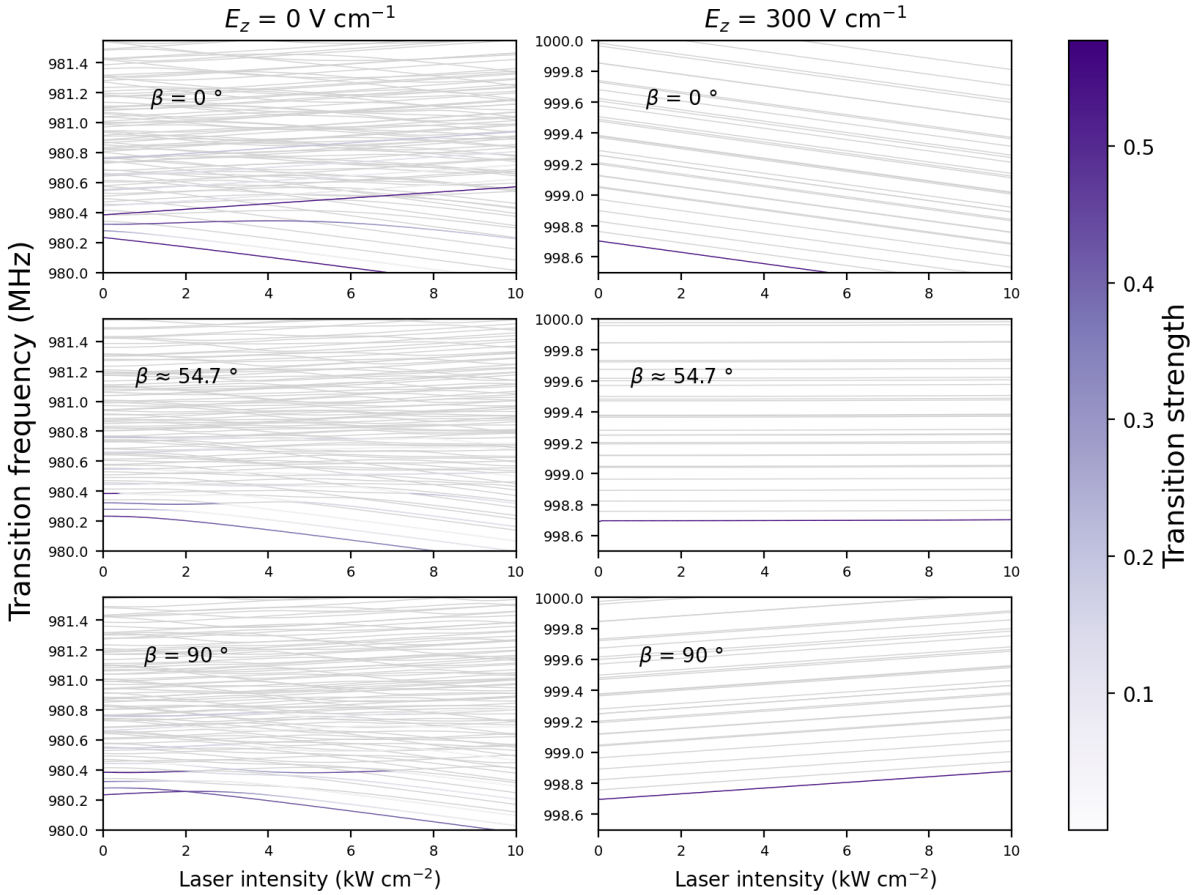

FIG. 5: RbCs in AC electric field as laser intensity increases a)0DC field, b)300v/cm DC field. When there is an external field, the molecule orientation is well defined so the use of magic angles can be exploited.

operator:

$$\hat{R}(\theta) = \begin{pmatrix} \cos\frac{\theta}{2} - i\frac{\Delta}{\Omega_{eff}}\sin\frac{\theta}{2} & -i\frac{\Omega}{\Omega_{eff}}e^{-i\phi}\sin\theta/2 \\ -i\frac{\Omega}{\Omega_{eff}}e^{+i\phi}\sin\theta/2 & \cos\frac{\theta}{2} + i\frac{\Delta}{\Omega_{eff}}\sin\frac{\theta}{2} \end{pmatrix}, \theta = \Omega_{eff} \cdot t_{pulse} \tag{14}$$

The proportion of the population that can be transferred to the excited state greatly decreases as the detuning of the radiation is increased from resonance so the energy structure of the system should be well understood and ways to minimise any fluctuations should be considered. The field detuning restricts the fidelity of any transitions so an energy structure that is minimally sensitive to external fields fluctuations should be used.

7. BLOCH SPHERE

Any two-level system can be written as $|\Psi\rangle = a\,|0\rangle + b\,|1\rangle$ with a,b being equal to complex numbers. The probability to detect either state is given by the square of the magnitude of these coefficients by Born's rule. By separating the complex coefficients into their phase and magnitude, $|\Psi\rangle = e^{i\alpha}(a\,|0\rangle + e^{i\varphi}b\,|1\rangle)$ the global phase, α, and the relative phase ,φ, are found.When

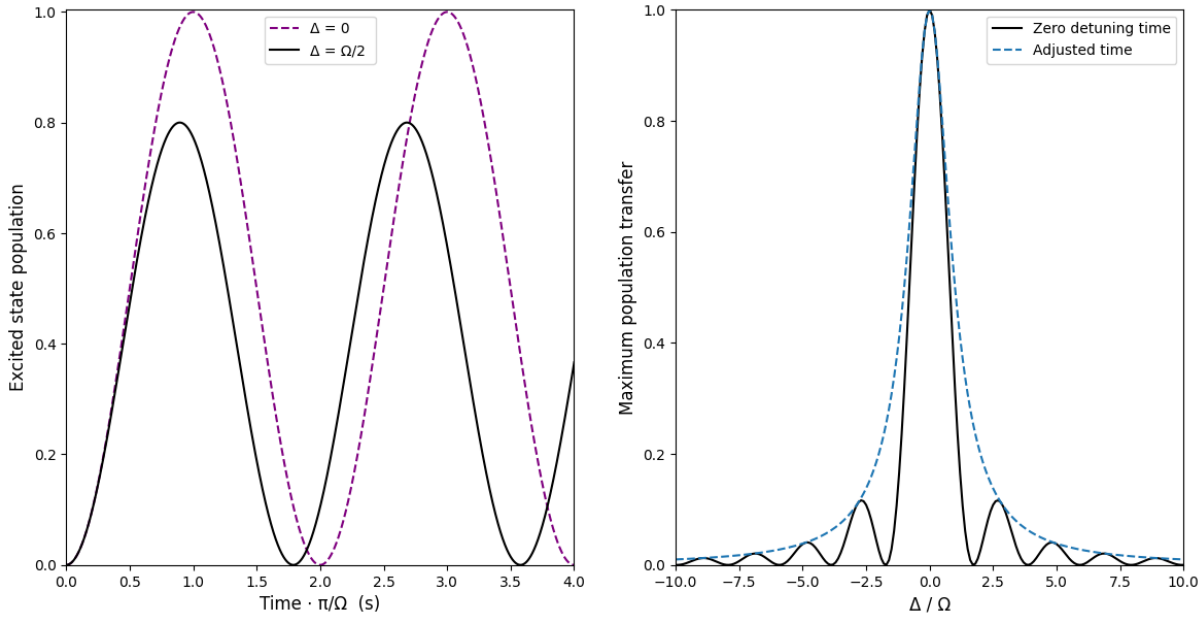

FIG. 6: 2 level Rabi oscillations. When resonant the Population cycles between either state. The effective Rabi frequency increases when detuned above or below resonance. When detuned the fraction of the population transfer becomes less efficient and sharply decreases the further from resonant as detuning increases.

initialised in a single state at the start of an experiment, in a rotating frame or interaction picture this relative phase will be between the molecule transition frequency and the field. The global phase can be dropped leading to: $|\Psi\rangle = (a|0\rangle + e^{i\varphi}b|1\rangle)$.Finally, since $a^2 + b^2 = 1$ to be normalised, the wavefunction can be wrote as:

$$|\Psi\rangle = \mathbf{cos}\frac{\theta}{\mathbf{2}}|0\rangle + e^{i\varphi}\mathbf{sin}\frac{\theta}{\mathbf{2}}|1\rangle\,. \tag{15}$$

Now the system can be fully described with only two variables θ and φ. Theta and phi can be used as spherical coordinates and any wavefunction will be represented as a point on a sphere of a constant radius since the magnitude of the wavefunction is always fixed to one. When applying a field the importance of the driving field phase is clear when considering how the Bloch vector evolves during a pulse. When the field is on the Bloch vector rotates around an axis given by the unit vector, where ϕ is the phase of the field[40]:

$$\hat{n} = \frac{1}{\sqrt{\Omega^2 + \Delta^2}}[\Omega cos(\phi), \Omega sin(\phi), \Delta] \tag{16}$$

ϕ can also depend on the molecules position $\phi = \phi_0 + k \cdot r$ which can cause problems when the molecule moves.In this report the effect of the motion on the phase is ignored. The importance of the phase can be seen on the Bloch sphere by plotting π pulses with different phases as seen in figure 7. Since the pulses are resonant, at any time in the duration of the two pulses, the amplitude of the state coefficients are equal and only differ by the relative phase, when only applying one pulse the phase is not important.

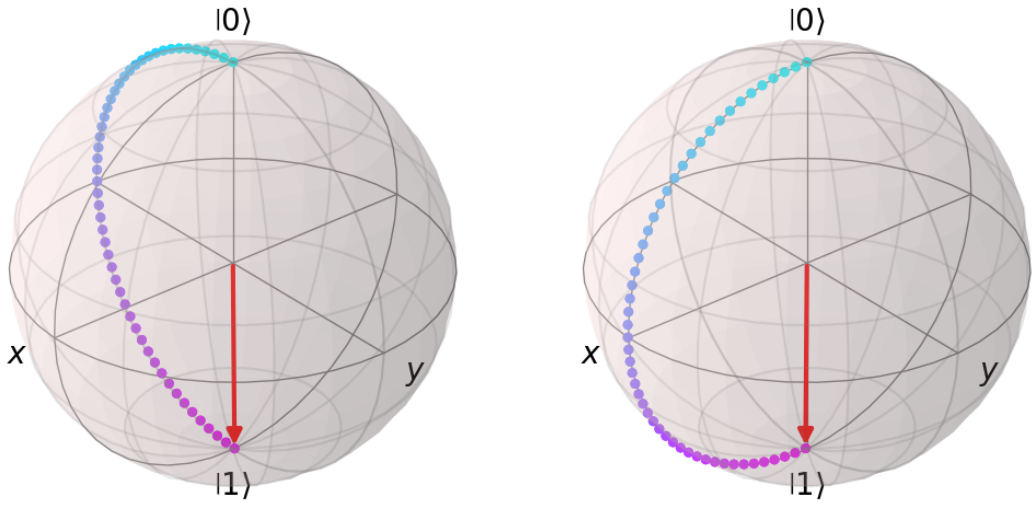

FIG. 7: The left Bloch sphere shows a driving field of initial phase zero. The right sphere has a driving field of phase 90 degrees. The evolution of the Bloch vector during the different π pulses shows the effect the field phase has on the relative phase of the superposition.The molecule is initialised fully in the ground state. Each point is equally spaced in time. The pulses are resonant so the population fully flips between states.

8. 3 LEVEL RABI OSCILLATIONS

Even when the applied field is resonant to a single state, any other transitions that have a similar transition frequency can be driven and start to introduce errors.For simplicity it is assumed that the excited state always transfers back to the initial ground state and does not couple to other lower rotational states. The simplest way to model this scenario is a 3-level system in a 'Vee' shape [19]. This is a 3 level system with one ground state and two excited states. Transitions between the two excited states are forbidden.The EM field applied is resonant on one transition and detuned on another. For this 3-level system made up of a ground state and two excited states it can be modelled by:

$$H_{Vee} = \frac{\hbar}{2}\begin{pmatrix} 2\Delta_1 & -\Omega_1 & 0 \\ -\Omega_1 & 0 & -\Omega_2 \\ 0 & -\Omega_2 & 2\Delta_2 \end{pmatrix}, |a\rangle = \begin{pmatrix} 1 \\ 0 \\ 0 \end{pmatrix}, |b\rangle = \begin{pmatrix} 0 \\ 1 \\ 0 \end{pmatrix}, |c\rangle = \begin{pmatrix} 0 \\ 0 \\ 1 \end{pmatrix} \tag{17}$$

By using a small scale for the time steps the exponential solution of the time evolution can be approximated:

$$i\hbar\frac{\partial\Psi}{\partial t} = H_{Vee}\Psi, \tag{18}$$

$$\Psi(t+dt) \approx (1-\frac{i}{\hbar}H_{Vee}dt)\Psi(t), \tag{19}$$

any fluctuations in detuning or field strength can be added at each step. In the appendix a method for choosing a time step size is shown. To model a specific scenario the 3rd level used

should be the closest excited state as the closest state will be driven with a smaller detuning so it's presence causes a larger effect. For this work the energy splitting between the two excited states is varied so that the results can be applied to any scenario. To test when the two level approximation is valid, applying a pulse using the time $t = \pi/\Omega$ whilst varying the energy splitting between target state $|a\rangle$ and the third state $|c\rangle$. When the two level approximation works well the coefficient of state $|a\rangle$ should be close to 1 since the pulse applied is a π pulse in the 2 level approximation. From figure 9, this method finds a limit on the Rabi frequency that can be used for a given energy splitting.

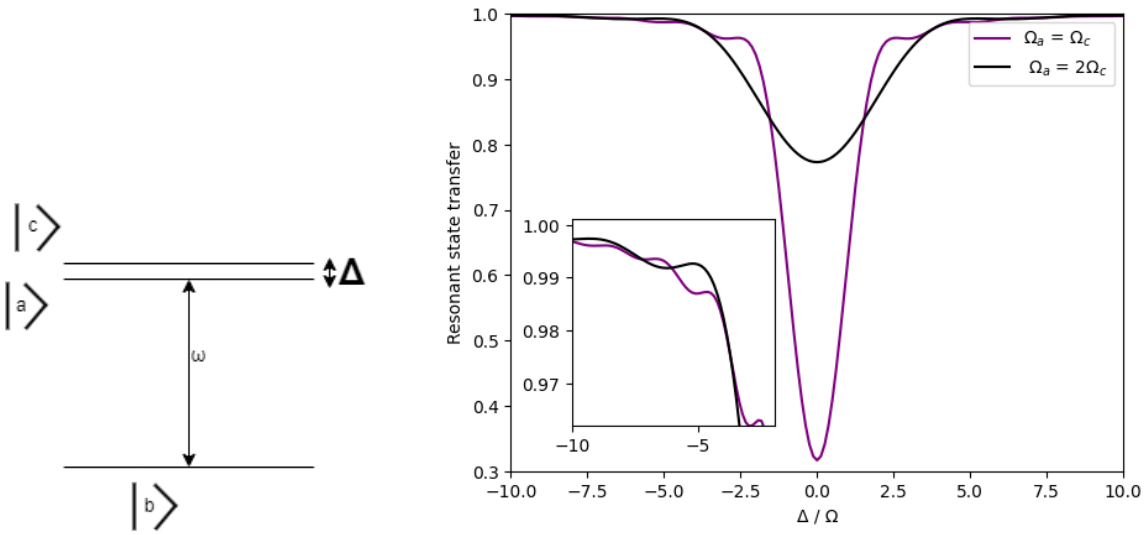

FIG. 8: 3 Level system energy structure

The quality of transitions to a target state can be improved by lowering the field strength of the laser. However, this can cause problems when using low field Rabi frequencies since the pulse times may become too slow compared to other effects such as the molecule or laser trap lifetime and these place an upper limit on the pulse time available. Although a higher field strength gives a lower proportion transferred, figure 6 shows using a higher Rabi frequency makes the effects of detuning less relevant. This idea should be able to be extended for when there are more than two available transitions to model specific molecules to find a limit on the Rabi frequency that can be used.

9. RAMSEY INTERFEROMETRY

The method know as Ramsey Interferometry was introduced In 1950. It showed that using 2 separated oscillating fields to drive transitions can give smaller half-widths on resonances and reduce the errors from non-uniform fields from previously used methods. In modern experiments the pulses can be separated in time rather than space due to the use of optical traps and ultracold temperatures. The first $\frac{\pi}{2}$ puts the molecule into an equal superposition state, if the field is resonant to the transition then no phase will accumulate between the molecule and the

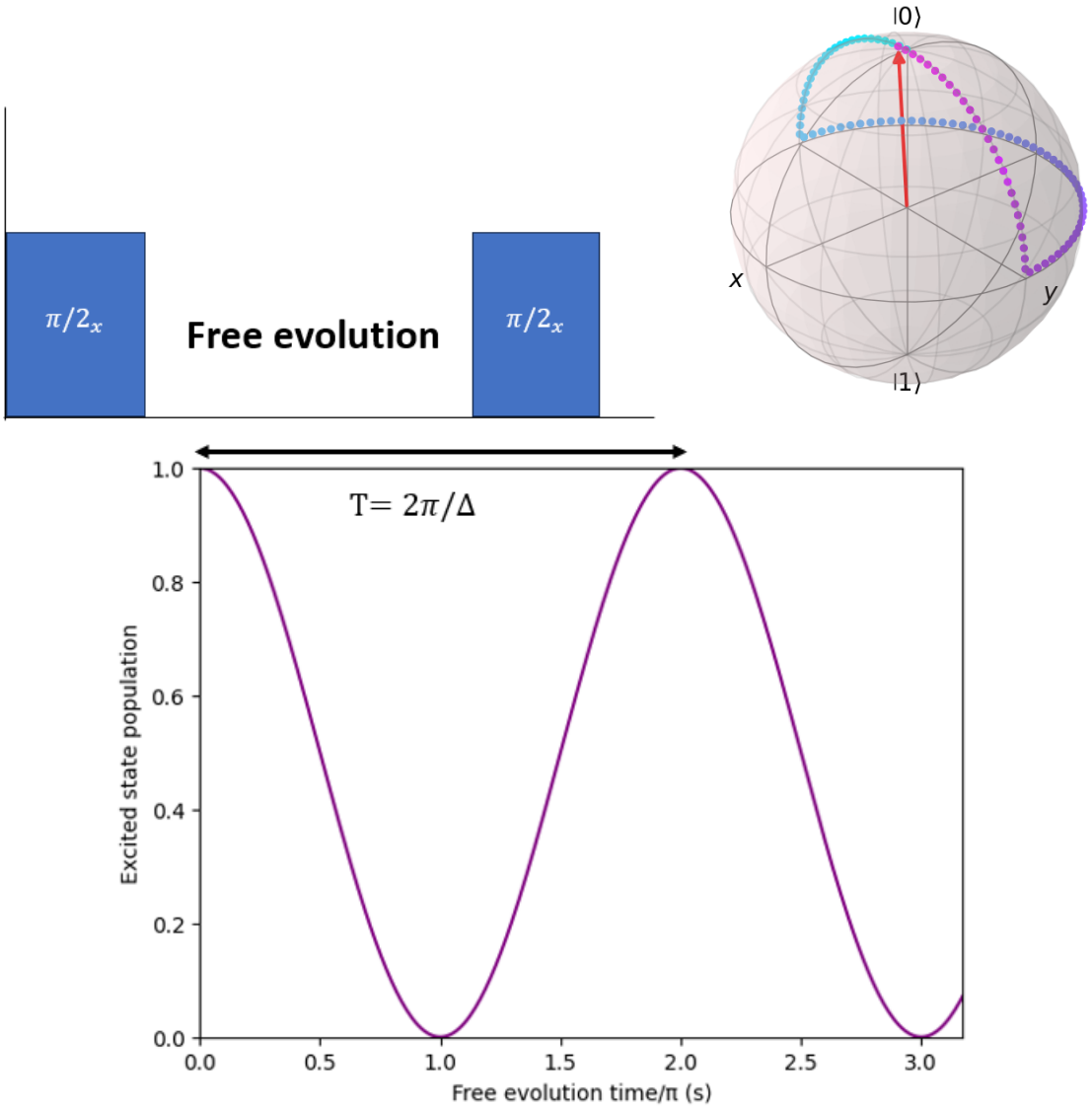

FIG. 9: Diagram of the pulse sequence used in a standard Ramsey experiment.When there is no free evolution time the two $\frac{\pi}{2}$ pulses should act as a π pulse. By varying the time between the two pulses the effects of dephasing can be investigated. The fringe oscillations are spaced proportional to the detuning, in this scenario plotted the detuning is small compared to Rabi frequency so the oscillations have a magnitude of approximately 1 since with no dephasing the population nearly fully transfers.Bloch sphere image shows how the Bloch vector evolves during the Ramsey experiment. The Bloch vector plotted shows the free evolution time = $\frac{\pi}{\Delta}$.

field during the free evolution. The free evolution can be described by the operator:

$$U = \begin{pmatrix} e^{i\Delta t/2} & 0 \\ 0 & e^{-i\Delta t/2} \end{pmatrix}, U = e^{i\Delta t/2} \begin{pmatrix} 1 & 0 \\ 0 & e^{-i\Delta t} \end{pmatrix}. \tag{20}$$

Since only the relative phase is important the global phase can be factored out to show how the relative phase accumulates more clearly. If the field is resonant the detuning will be zero so no phase develops when the field is turned off. On the Bloch sphere, the pulse sequence

is represented by 3 separate rotations. For a molecule fully prepared in the ground state, the Bloch vector points up the z-axis. The first pulse rotates the Bloch vector around the x-axis to the equator and the molecule is then in an equal superposition. Then during the free evolution, the Bloch vector rotates around the equator. The second pulse rotates the Bloch vector around the x-axis again and the final state depends on the amount of rotation around the z-axis. When repeating the experiment many times and varying the free evolution time the final output state will oscillate between the two states at a rate proportional to the detuning. When this experiment is done on many molecules at once there will be a distribution of detuning's from the molecule motion, interactions with the environment and any non-uniform external fields. The distribution of the detuning can be modelled by a normal distribution and for simulations a detuning is sampled from that distribution. When performing a Ramsey experiment on all the molecules, each molecule will dephase at a different rate during the free evolution due to the differences in detuning. After repeating the experiment over different free evolution times the effects of the different phases can be seen since the number of molecules in the excited state will decays until long evolution times where the phases are randomised and the amount of molecules measured in a state will be half. This is represented on the Bloch sphere by taking the average of the individual Bloch vectors. For long times between the pulses the molecule phases are randomly distributed so then the probability of measuring the either state is a half. The time for average number of molecules in the excited state to decay by a factor of e is called the $1/e$ coherence time. By varying the width of the normal distribution that the detunings are sampled from the relation between the $1/e$ coherence time and detuning can be investigated. The mean detuning was set to zero so that there is no fringe oscillations making the curve fitting easier. To get the coherence time a chi-squared method was used that fitted the curve:

$$y = \frac{1}{2}\exp\left(-\frac{x}{t}\right) + \frac{1}{2}, \tag{21}$$

with t being the coherence time. The relation between the standard deviation of the detuning distribution and the coherence time shows the importance of minimising any unwanted interactions since the coherence time is a measure of how long the superposition can be kept isolated from the environment. For each detuning distribution width the Ramsey experiment was repeated 500 times and then averaged to get a normalised excited state population for each free evolution value. The errors on the results used were the standard error and were used for fitting the coherence time. In the logarithmic scale, a linear model was fitted to the coherence times and the resulting gradient was -1.012 $\pm$ 0.006626 and an intercept of 0.1101 $\pm$ 0.007308 which equates to a relation of:

$$T = \frac{10^{0.1101}}{\Delta^{1.012}}, \tag{22}$$

Showing that they are approximately inversely proportional.

10. EXTENDING COHERENCE TIME

To overcome the effect of dephasing, different pulses can be applied during the free evolution to cause the phases to realign at a later time. In 1950 Erwin Hahn used a π pulse to undo the dephasing caused by the different precession rates of spins in a non-uniform magnetic field.

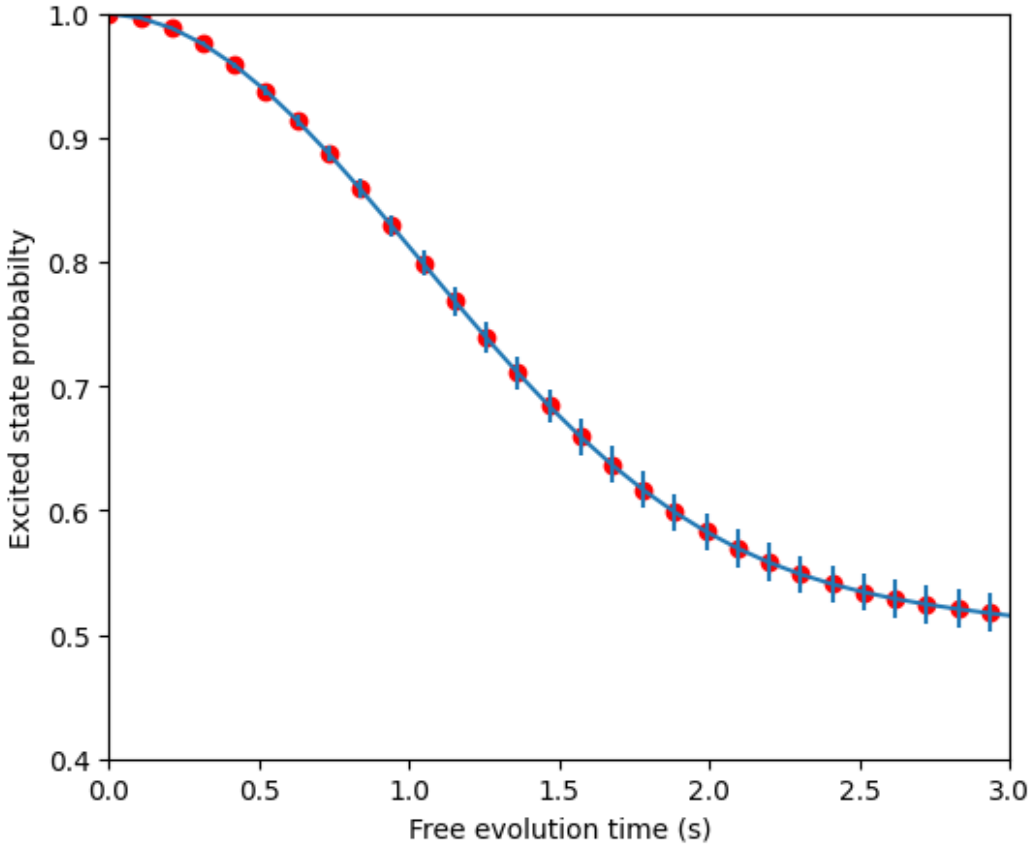

FIG. 10: Ramsey experiment averaged over 500 molecules with the detunings sampled from a distribution with a standard deviation of 1Hz. At approximately 1 second the excited state population factor has decayed by a factor of e so the coherence time is close to 1 second. The errors become larger for longer times due to the molecules starting to rephase and constructively add due to the finite number of them.

In an ideal scenario the precession rates differ but are fixed so when the π pulse is applied halfway during the free evolution all the spins should align back. If the detuning varies during the free evolution the phase accumulated before and after the pulse will differ so that the pulse improves coherence but does not fully correct the dephasing. This technique is commonly called a spin echo or Hahn echo since the rephasing of the spins causes an 'echo' of a current signal in the NMR machine. By applying multiple pulses the free evolution time can be split into smaller sections so that the phase accumulated from each section is closer to constant so that the effects of dephasing is more effectively removed. However, when detuned the effects of pulse imperfections accumulate and can become more of a problem than the dephasing.

11. COMPOSITE PULSES

By combining pulses of different initial phases into sequences more robust pulses can be made to overcome the effects of detuning and time errors on the population transfer. The different phases correspond to different rotation axis on the Bloch sphere and combining these in a sequence can undo the effects a detuned pulse which causes a rotation around the z-axis. The

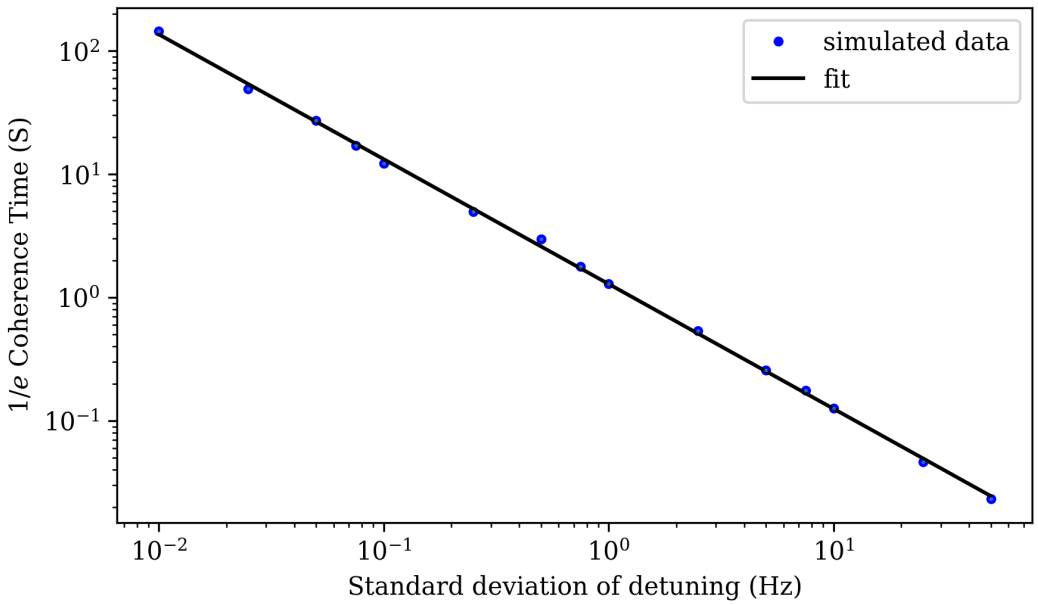

FIG. 11: Trend of the coherence time fitted whilst varying the detuning distribution width. On the log scale the relationship is linear with a gradient of -1.012 $\pm$ 0.006626 meaning that they are approximately inversely proportional. The smaller light blue points inside the larger dark blue points are the error bars but are barely visible when put into the log scale.

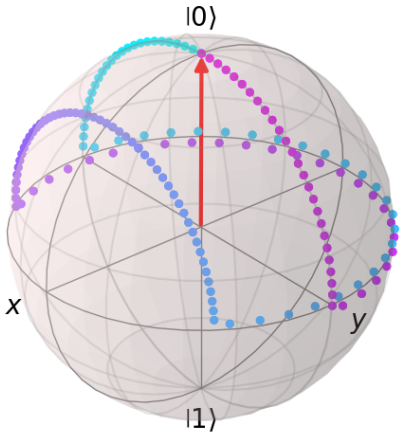

FIG. 12: Evolution of the Bloch vector in a Ramsey experiment with a π pulse applied halfway during the free evolution. Since the detuning is constant the π pulse fully removes the dephasing effects. The overall flip angle of the sequence is 2π so the Bloch sphere shows the expected result as if no dephasing occurred.

simplest composite pulse that makes use of different rotation axis is the XY4 sequence. The Knill pulse is a composite sequence that can be used to replace π pulses in cyclic sequences - a pulse sequence that contains an even amount of π pulses - to make them more robust. For example, the XY4 sequence's performance under errors can be improved by replacing each pulse by Knill pulses since it has an even number of pulses. The spin echo sequence cannot be replaced

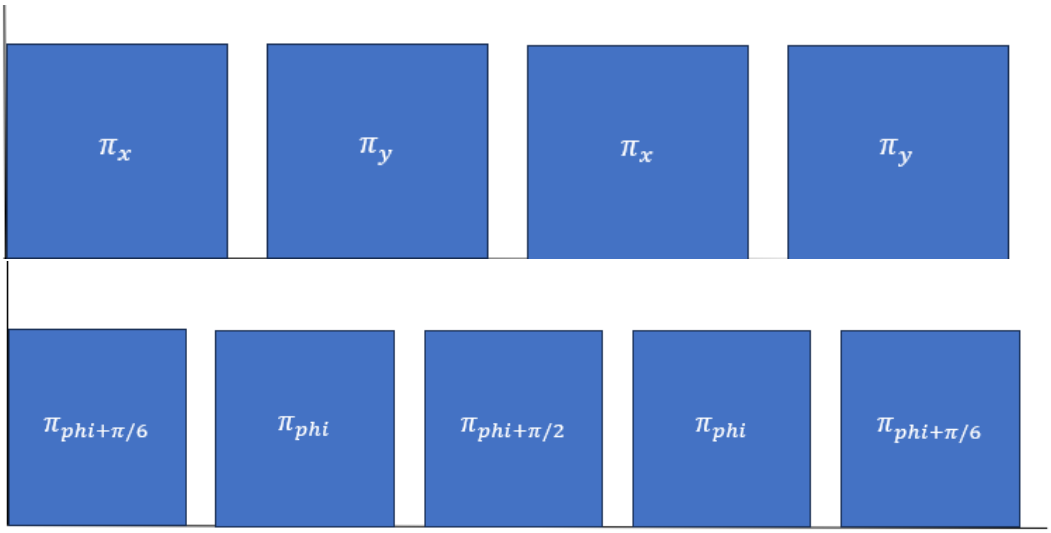

FIG. 13: Pulses used to make the XY4 and Knill pulse. The lower index shows the phase of the individual pulses. The overall rotation for the XY4 sequence is 4π and the molecule is returned back to it's original state after the pulse sequence. The Knill pulse contains 5 π pulses so the state is changed after the sequence. Phi refers to the overall phase - rotation axis on the Bloch sphere - of the Knill sequence.

by a Knill pulse since it has an odd number of pulses however applying spin echo twice could be replaced. To investigate the performance of the pulse sequences can be applied while the detuning and time errors of each individual pulse are varied. Alternatively Average Hamiltonian Theory can be used to model the pulses as operators then separating them into error terms and an ideal pulse operator:

$$e^{H_{eff}} = e^{H_{errors}} e^{H_{ideal}} e^{H_{errors}} \tag{23}$$

[37, 39]. Using this method, the XY4 sequence is shown to be the simplest sequence that removes the zero-order average Hamiltonian for a general dephasing environment and [37] shows that reapplying the sequence which is known as XY8 reduces higher order pulse errors. The Knill pulse removes the first-order average Hamiltonian and higher orders are kept small [38]. In the appendix, it is shown why the Knill pulse has to be used in cyclic sequences and the rotation matrix for an XY4 pulse is given. These composite pulse sequences do not correct for an arbitrary initial state so the use in an experiment is limited by how well the molecules are prepared before the pulse sequence is applied. For performing Ramsey experiment this means an error tolerant $\frac{\pi}{2}$ pulse is needed to start the sequence so that errors do not accumulate. Composite pulses that allow for variable flip angles [35] were also simulated to test their performance. Since these pulses are less robust than XY4 and the Knill pulse, Ramsey interferometry is limited by the composite $\frac{\pi}{2}$ pulses. The BB1 and BB2 pulse were tested by applying them twice to mimic how they would be used in a Ramsey experiment whilst the other composite pulses were applied between two perfect $\frac{\pi}{2}$ pulses that had no time or detuning errors.

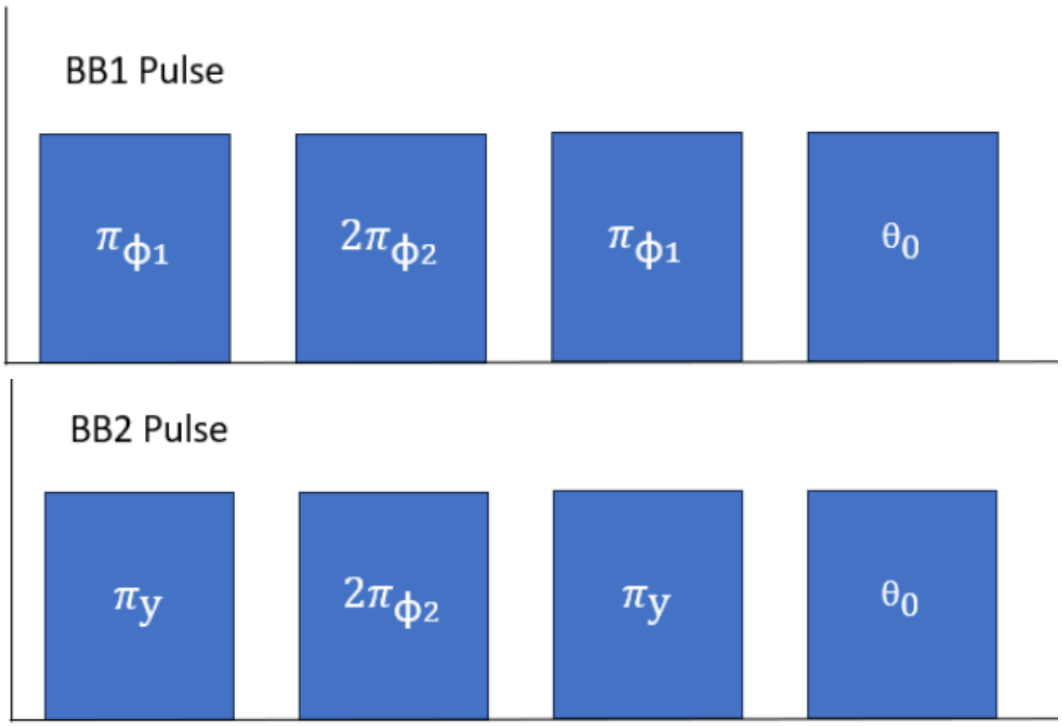

FIG. 14: BB1 and BB2 are composite pulses that have a variable flip angle. For both pulses θ represents the total flip angle. For the context of this report they are used to replace the $\frac{\pi}{2}$ pulses so $\theta = \frac{\pi}{2}$. ϕ_1 for BB1 is $\arccos(\frac{\theta}{4\pi})$ and $\phi_2 = 3\phi_1$. For the BB2 sequence, $\phi_2 = \frac{3}{2}\pi + \frac{\theta}{4}$

A. 3 level composite pulses

Until now, in the previous section the composite pulses were only tested on the ideal 2-level system but for RbCs in the absolute GS, there are up to 5 different rotational states it could couple to when driven with a certain polarisation. To further test how well the composite pulses work without only 2 levels, they were simulated on a 3-level system in the limit that the Rabi frequency is much smaller than the energy splitting. The pulses were tested using a $\Omega = \Delta/10$ and detuning on the target state equal to 5% of the Rabi frequency so that it is in the region where the 2-level approximation is valid to use.

12. DYNAMICAL DECOUPLING

Using composite pulses for decoupling allows for the pulses to be reapplied without the effects of pulse errors accumulating to extend the coherence time further. The best decoupling sequences depends of the type of errors that have to be removed but this report focuses only on pure dephasing. In general, rotations around different Bloch sphere axis should be used [34] however for pure dephasing noise regular π pulses can fully undo the system-environment interaction. Pure dephasing noise can be modelled by the Hamiltonian:

$$H = \frac{\hbar}{2}\begin{pmatrix} \beta(t) & 0 \\ 0 & -\beta(t) \end{pmatrix}, \tag{24}$$

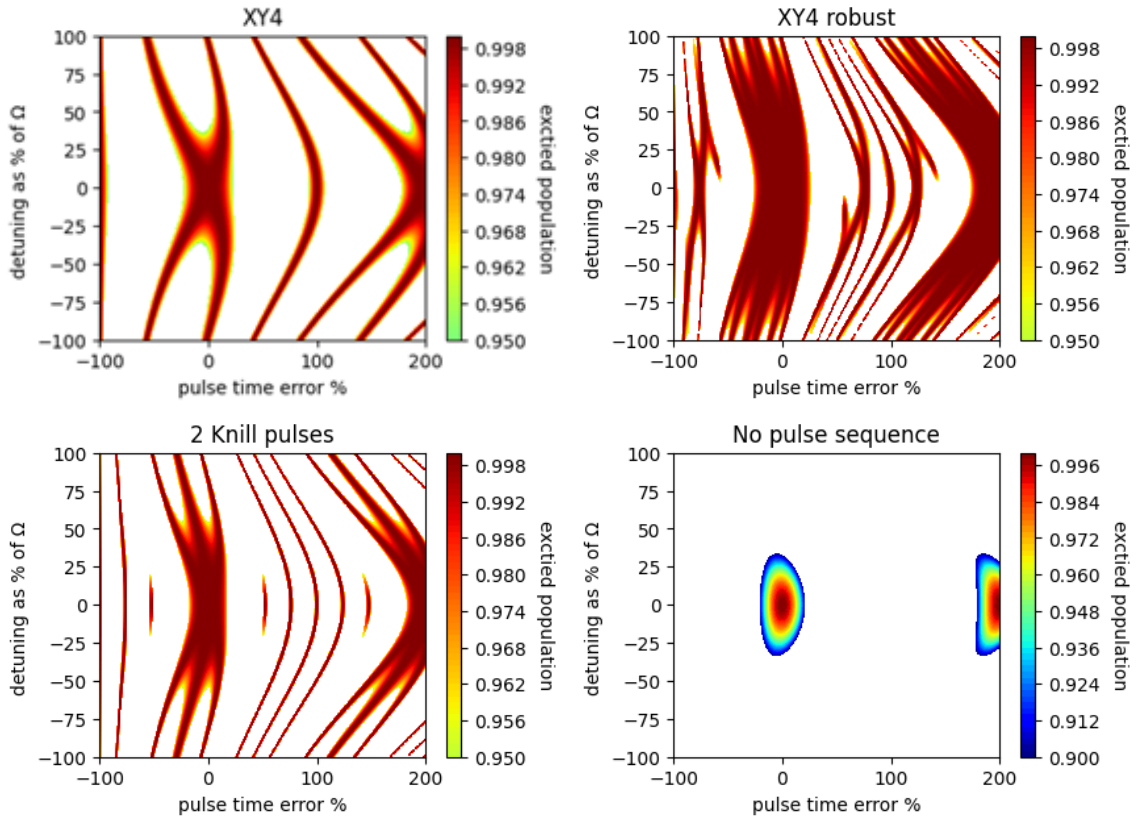

FIG. 15: Pulse performance under detuning and time errors. The composite pulses were tested by inserting them in a Ramsey sequence where the $\frac{\pi}{2}$ pulses were assumed to be perfect so that the errors measured are only from the pulse sequence. The XY4 robust sequence is the XY4 pulse with each pulse replaced by a Knill pulse showing how combining pulse can be made for more robust sequences.

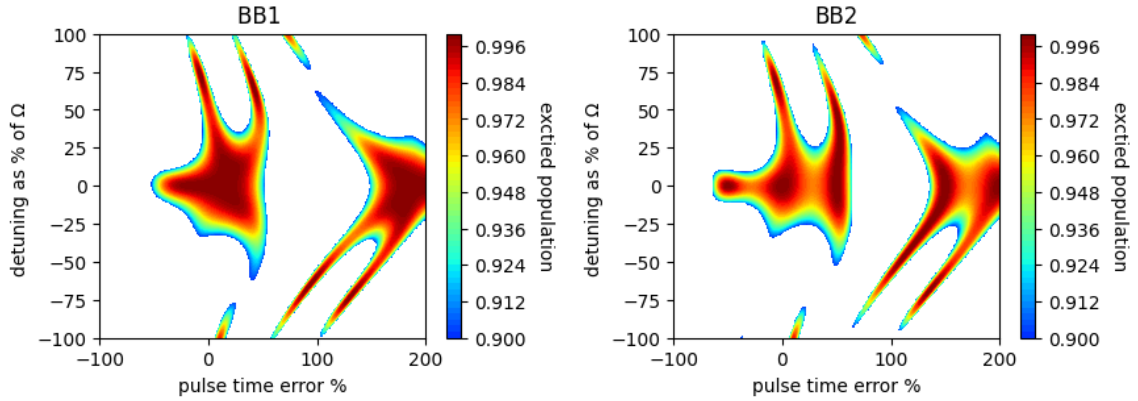

FIG. 16: The variable flip angle composite pulses were tested by applying them twice under detuning and time errors to mimic their use in a Ramsey sequence.

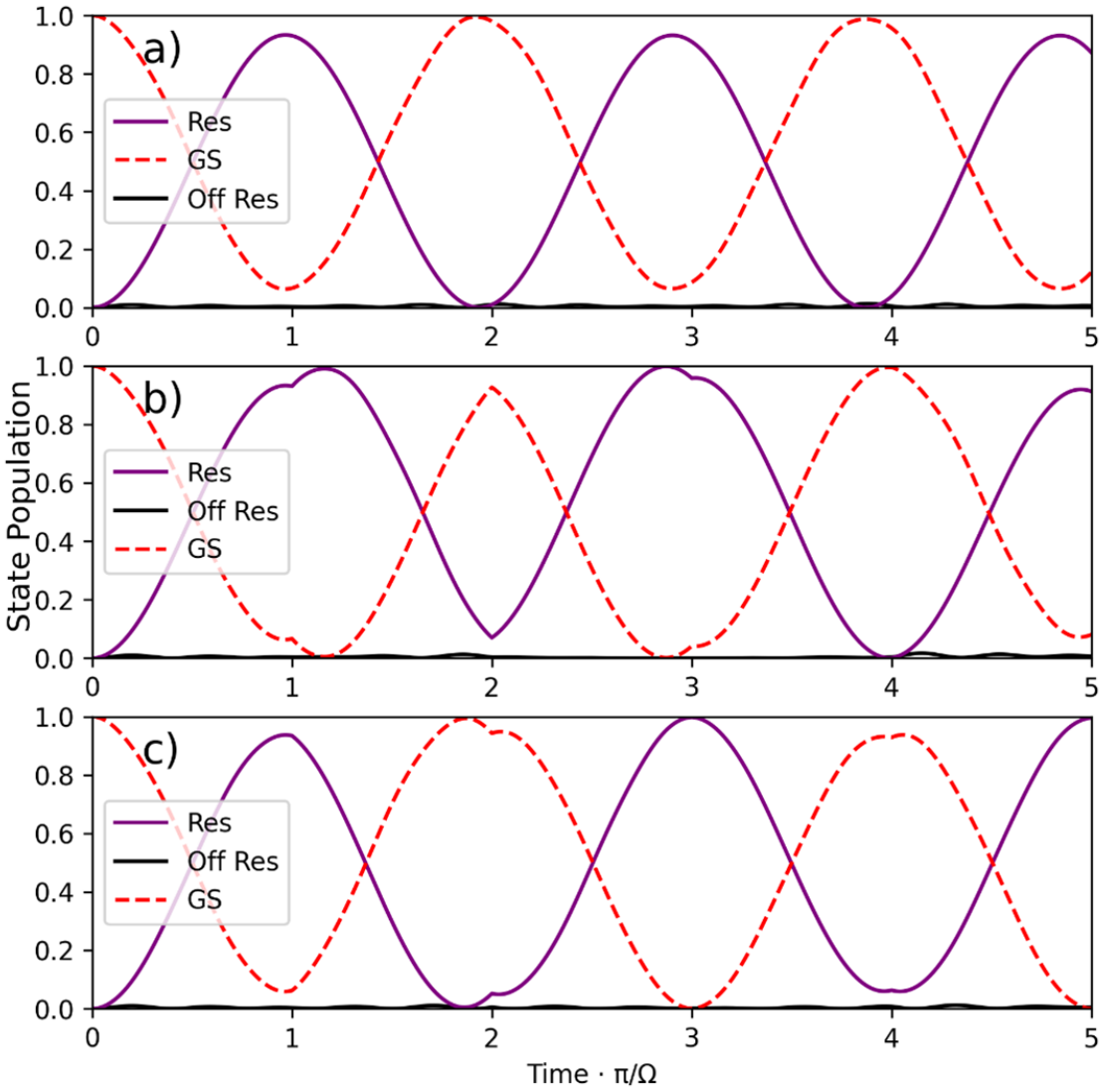

FIG. 17: Composite pulses tested in the 3 level system. a) Regular pulse applied b) XY4 sequence applied, at $t = 4\pi/\Omega$ the sequence finishes and the molecule is back to it's initial state. The sequence corrected for detuning adn time errors better than the regular pulse. c) Knill pulse applied at $t = 5\pi/\Omega$ the population has flipped and shows the result of a robust π pulse.

which would represent changes in the transition frequency/detuning during an experiment. Now, during the free evolution the phase accumulated can be found from the operator:

$$U = \begin{pmatrix} e^{i\frac{\int \beta(t)dt}{2}} & 0 \\ 0 & e^{-i\frac{\int \beta(t)dt}{2}} \end{pmatrix}, \tag{25}$$

where the time integral is over the free evolution period. By tracking the phase accumulated in a Ramsey experiment after applying n pulses around the y-axis on the Bloch sphere represented

by the operator:

$$U = \begin{pmatrix} 0 & -i \\ i & 0 \end{pmatrix}. \tag{26}$$

the phase at the end of the free evolution is given by[33]:

$$\widetilde{\phi} = (-1)^n \int_{t_{n-1}}^{t_n} \beta(t)dt... + \int_{t_1}^{t_2} \beta(t)dt - \int_{t_0}^{t_1} \beta(t)dt, \tag{27}$$

since the effect of the pulses acts as reversing the phase accumulation. The direction of the phase accumulation is flipped after each pulse and shows that if the background noise $\beta(t)$ is nearly constant that one pulse will completely undo the phase accumulation agreeing with spin echo results. By applying more pulses the free evolution is split into separate periods of alternating signs which allows fluctuating background noise to be reduced. By transforming the system-environment noise to the power spectral density:

$$S_\beta(\omega) = \int_{-\infty}^{\infty} e^{i\omega\tau} \langle \beta(t)\beta(t+\tau) \rangle d\tau, \tag{28}$$

the coherence can be shown to be:

$$\frac{2}{\pi} \int_0^{\infty} \frac{S_\beta(\omega)}{\omega^2} F(\omega\tau), \tag{29}$$

where $F(\omega\tau)$ is known as the filter function and depends on the number of pulses and their timings. The overlap between the filter function and the spectral density of the background noise then defines the coherence after a pulse sequence.

A. Filter Function

The filter function can be shown to be[33]:

$$F(\omega\tau) = |1 + (-1)^{n+1} e^{i\omega\tau} + 2\sum_{j=1}^{n} (-1)^j e^{i\delta_j \omega\tau}|^2, \tag{30}$$

and shows the effectiveness of a pulse sequence can be changed by varying the pulse times rather than applying more pulses. When the specific spectral density for a system is known or can be approximated then a optimal pulse timing can be found by minimising how it overlaps with the filter function. Although the derivation only considers pulses around one axis, the XY4 pulse was used in the comparison for decoupling with different pulse timings.By taking the time derivative of the filter function, the pulse timings of an n-pulse sequence that minimise it for ω around zero can be found and result in pulse times at [34,33]:

$$t_j = sin^2 \left(\frac{j\pi}{2(n+1)} \right), \tag{31}$$

for the rest of the report these pulse times are called sine spacing. Alternatively the sine spacing can be thought as suppressing the first n terms of the Taylor expansion of $\beta(t)$[36]. Since only

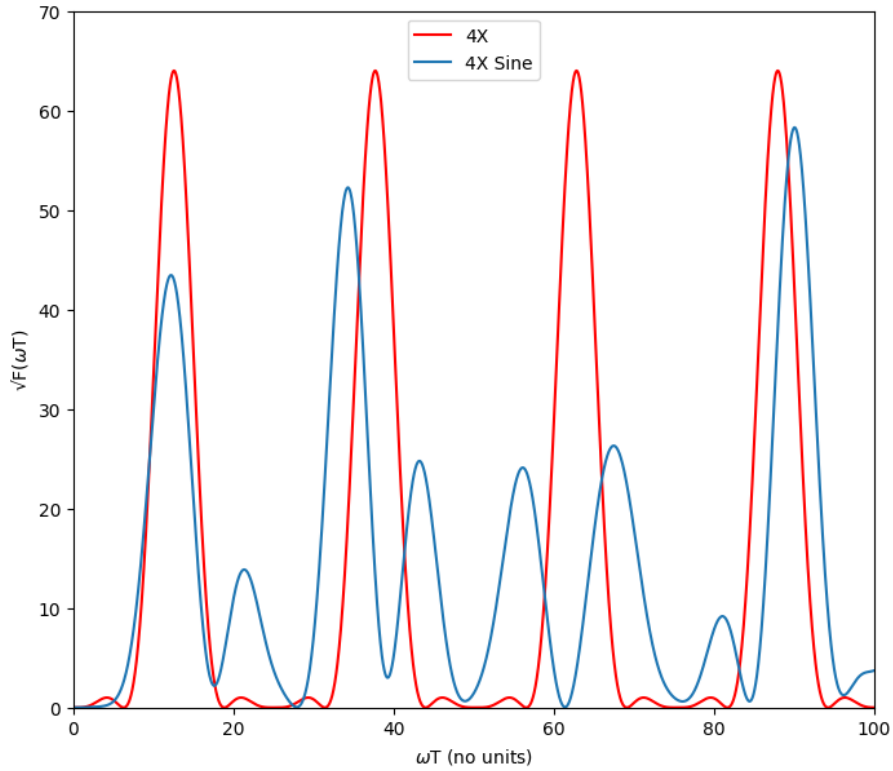

FIG. 18: Graph shows the square root of the filter function for a 4 pulse sequence for the equal spacing and sine spacing times. Both filter noise but the since spacing is minimised around $\omega = 0$. The effectiveness of either pulse sequence will depend on the spectral density of the background noise and will be depend on the experiment.

the effectiveness of decoupling is wanted to be investigated, the Ramsey sequences are started by using resonant $\frac{\pi}{2}$ pulses. For ω = 4 the sine spacing of the XY4 and π pulses extends the coherence time compared to the equal time spacing. However, the regular π pulses accumulate errors so a composite pulse sequence should be used. A detuning distribution width of 15Hz which is 15% of the Rabi frequency was used so that the effects of pulse errors were clear.

TABLE I: $1/e$ Coherence time fitted to the decay of the state population when the detuning fluctuates 4 times during the experiment

Pulse sequence	Coherence time (s)	Error (s)
XY4 sin	2.8680	$2.513 \times 10^{-}2$
XY4	0.6146	$6.371 \times 10^{-}3$
Spin echo	0.5211	$4.521 \times 10^{-}3$
X4 sin	1.7840	$3.301 \times 10^{-}2$
X4	0.5675	$2.941 \times 10^{-}3$
No pulse	0.08316	-

The coherence time for no pulse sequence was calculated using equation 22 so there is no error from fitting. The XY4 sine spacing sequence gives a coherence time approximately five times longer than it's equal spaced time sequence and shows the effectiveness of considering the timing of pulses. Applying 4 pulses of the same phase were shown to improve the coherence time however the pulse errors accumulate quickly so the need for the composite pulses is clear. The XY4 robust pulse sequence was not tested but will improve the coherence by being much more robust. It also consists of 20 pulses which causes the filter function to filter out better for lower ω.

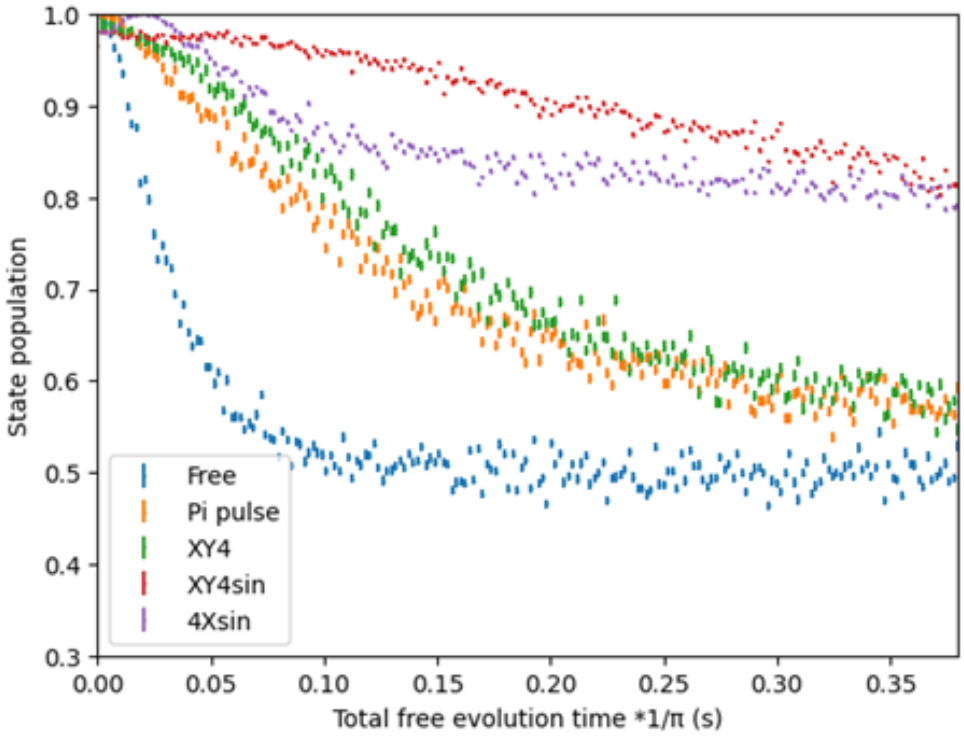

FIG. 19: Effectiveness of different decoupling sequences tested when the detunings fluctuates at 4 equally spaced times during Ramsey interferometry (each 0.2 seconds for a free evolution length of 1 second). Using the same pulse sequence but with different pulse timings can greatly change the effectiveness as seen by the XY4 sequence and the 4π pulse sequence.

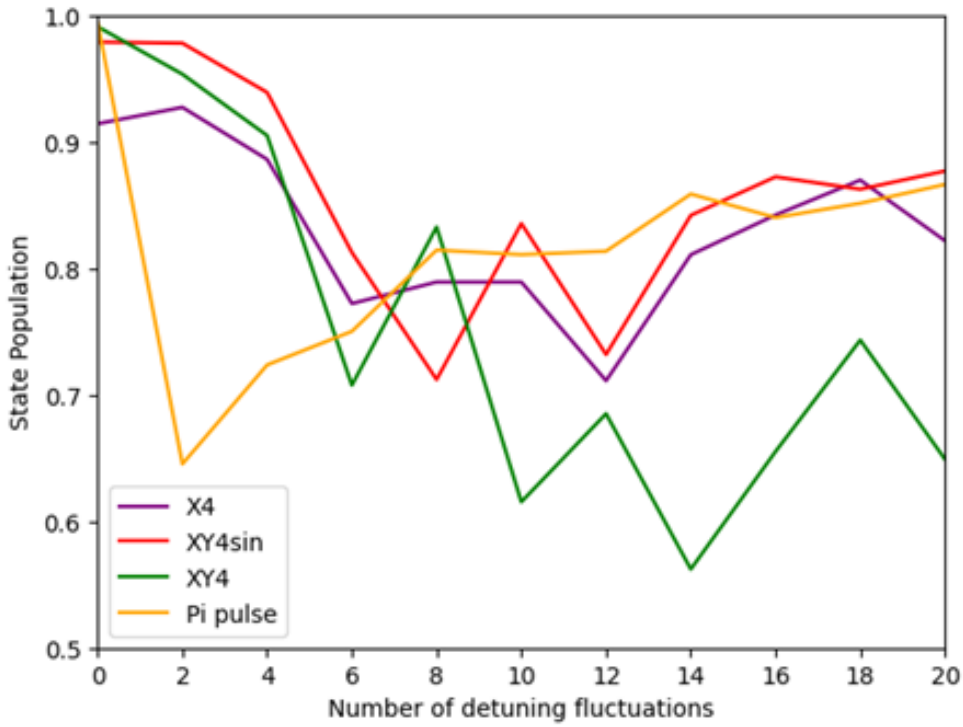

FIG. 20: By changing the number of fluctuations of the detuning and fixing the evolution time during Ramsey interferometry the different pulse sequences can be seen to perform differently. An evolution time of 1 second was used and the standard deviation of the detuning was 15Hz. The average of 500 runs was used for each value. For no fluctuations, all pulses remove the dephasing effect but pulse imperfections accumulate.

13. FUTURE WORK

The effects of different detuning during a composite pulse were not looked at in depth. However, when they were used in the decoupling sequences the composite pulses worked well under different fluctuation rates so their performance shouldn't drop significantly. By combining how different composite pulses act under different background noises with varied pulse timings optimal sequences could be found for specific experiments. Other methods for deriving robust pulses involve varying the Rabi frequency so that pulse area is constant but different shape [32] rather than the rectangular pulses only consider here:

$$\int_0^{T_{pulse}} \Omega(t)dt. \tag{32}$$

The pulse times for the filter function derivation were classed as 0 and for pulses that have a similar length to the evolution time, the majority of the dephasing will occur during applying the pulses so this effect needs to be considered as the filter function assumed the pulses were resonant and only consider detuning during the evolution time. The 3-level approximation used did not consider coupling to other ground states which may cause problems in experiments for molecules with small energy splitting. The effect of slight phase errors was not considered for pulse sequences around multiple axis and could be an area to look into for composite pulses.

REFERENCES

[1] Toscano, J., Lewandowski, H.J. and Heazlewood, B.R. (2020) 'Cold and controlled chemical reaction dynamics', Physical Chemistry Chemical Physics, 22(17), pp. 9180–9194. doi:10.1039/d0cp00931h.

[2] Ni, K.-K., Rosenband, T. and Grimes, D.D. (2018) 'Dipolar exchange quantum logic gate with polar molecules', Chemical Science, 9(33), pp. 6830–6838. doi:10.1039/c8sc02355g.

[3] DeMille, D. et al. (2008) 'Using molecules to measure nuclear spin-dependent parity violation', Physical Review Letters, 100(2). doi:10.1103/PhysRevLett.100.023003

[4] Fitch, N.J. et al. (2020) 'Methods for measuring the electron's electric dipole moment using ultracold YbF molecules', Quantum Science and Technology, 6(1). doi:10.1088/2058-9565/abc931.

[5] Gregory, P.D. et al. (2021) 'Robust storage qubits in ultracold polar molecules', Nature Physics, 17(10), pp. 1149–1153. doi:10.1038/s41567-021-01328-7.

[6] DeMille, D. (2002) 'Quantum computation with trapped polar molecules', Physical Review Letters, 88(6). doi:10.1103/physrevlett.88.067901.

[7] Blackmore, J.A. et al. (2018) 'Ultracold molecules for Quantum Simulation: Rotational coherences in CAF and RbCs', Quantum Science and Technology, 4(1), p. 014010. doi:10.1088/2058-9565/aaee35.

[8] Ketterle, W., Durfee, D.S. and Stamper-Kurn, D.M. (1999) Making, probing and understanding Bose-Einstein condensates . Contribution to the proceedings of the 1998 Enrico Fermi summer school on Bose-Einstein condensation in Varenna, Italy.

[9] Dulieu, O. and Gabbanini, C. (2009) 'The formation and interactions of cold and ultracold molecules: New challenges for interdisciplinary physics', Reports on Progress in Physics, 72(8), p. 086401. doi:10.1088/0034-4885/72/8/086401.

[10] Shor, P.W. (1997) "Polynomial-time algorithms for prime factorization and discrete logarithms on a quantum computer," SIAM Journal on Computing, 26(5), pp. 1484–1 509. https://arxiv.org/abs/quant–ph/9508027

[11] Li, Z. et al. (2017) High-fidelity adiabatic quantum computation using the intrinsic Hamiltonian of a spin system: Application to the experimental factorization of 291311. https://arxiv.org/abs/1706.08061

[12] Li, J.-R. et al. (2021) 'Tuning of dipolar interactions and evaporative cooling in a three-dimensional molecular quantum gas', Nature Physics, 17(10). doi:10.1038/s41567-021-01329-6.

[13] Żuchowski, P.S. and Hutson, J.M. (2010) 'Reactions of ultracold alkali-metal dimers', Physical Review A, 81(6). doi:10.1103/physreva.81.060703.

[14] Klein, J., Beil, F. and Halfmann, T. (2008) 'Experimental investigations of stimulated Raman adiabatic passage in a doped solid', Physical Review A, 78(3). doi:10.1103/physreva.78.033416.

[15] Vasilev, G.S., Kuhn, A. and Vitanov, N.V. (2009) 'Optimum pulse shapes for stimulated Raman adiabatic passage', Physical Review A, 80(1). doi:10.1103/physreva.80.013417.

[16] Blackmore, J.A. et al. (2023) 'Diatomic-Py: A python module for calculating the rotational and hyperfine structure of 1Σ molecules', Computer Physics Communications, 282, p. 108512. doi:10.1016/j.cpc.2022.108512.

[17] Blackmore, J.A. et al. (2020d) 'Controlling the AC stark effect of RbCs with DC electric and Magnetic Fields', Physical Review A, 102(5). doi:10.1103/physreva.102.053316.

[18] Atom-Light Interactions course by M. P. A. Jones

[19] Coleman, Z.C. and Carr, L.D. (2022) 'Exact analytical solution of the driven qutrit in an open quantum system: lambda and Vee configurations', Journal of Physics B: Atomic, Molecular and Optical Physics, 55(6), p. 065501. doi:10.1088/1361-6455/ac5efa.

[20] Li, J.-R. et al. (2023) 'Tunable itinerant spin dynamics with polar molecules', Nature, 614(7946), pp. 70–74. doi:10.1038/s41586-022-05479-2.

[21] Wolfowicz, G. and Morton, J.J.L. (2016) 'Pulse techniques for Quantum Information Processing', eMagRes, pp. 1515–1528. doi:10.1002/9780470034590.emrstm1521

[22] Uhrig, G.S. (2008) 'Exact results on dynamical decoupling by π pulses in quantum information processes', New Journal of Physics, 13(5), p. 059504. doi:10.1088/1367-2630/13/5/059504.

[23] Green, T.J. et al. (2013) 'Arbitrary quantum control of qubits in the presence of universal noise', New Journal of Physics, 15(9), p. 095004. doi:10.1088/1367-2630/15/9/095004.

[24] Souza, A.M., Álvarez, G.A. and Suter, D. (2011) 'Robust dynamical decoupling for Quantum Computing and Quantum Memory', Physical Review Letters, 106(24). doi:10.1103/physrevlett.106.240501.

[25] Biercuk, M.J., Doherty, A.C. and Uys, H. (2011) 'Dynamical decoupling sequence construction as a filter-design problem', Journal of Physics B: Atomic, Molecular and Optical Physics, 44(15), p. 154002. doi:10.1088/0953-4075/44/15/154002.

[26] J. M. Brown, A. Carrington, Rotational Spectroscopy of Diatomic Molecules (Cambridge Molecular Science), Cambridge University Press, 2010.

[27] Gregory, P.D. et al. (2019) 'Sticky collisions of ultracold RbCs molecules', Nature Communications, 10(1). doi:10.1038/s41467-019-11033-y.

[28] Hahn, E.L. (1950) 'Spin echoes', Physical Review, 80(4), pp. 580–594. doi:10.1103/physrev.80.580.

[29] Viola, L. and Lloyd, S. (1998) 'Dynamical suppression of decoherence in two-state quantum systems', Physical Review A, 58(4) doi:10.1103/physreva.58.2733.

[30] Uhrig, G.S. (2007) 'Keeping a quantum bit alive by optimized pulse sequences', Physical Review Letters, 98(10). doi:10.1103/physrevlett.98.100504.

[31] Götz S Uhrig 2008 New J. Phys. 10 083024 Exact results on dynamical decoupling by π pulses in quantum information processes doi: 10.1088/1367-2630/10/8/083024

[32] Kuzmanović, M. et al. (2024) 'High-fidelity robust qubit control by phase-modulated pulses', Physical Review Research. doi:10.1103/physrevresearch.6.013188.

[33] Biercuk, M.J., Doherty, A.C. and Uys, H. (2011) 'Dynamical decoupling sequence construction as a filter-design problem', Journal of Physics B: Atomic, Molecular and Optical Physics. doi:10.1088/0953-4075/44/15/154002.

[34] Souza, A.M., Álvarez, G.A. and Suter, D. (2012) 'Robust dynamical decoupling', Philosophical Transactions of the Royal Society A: Mathematical, Physical and Engineering Sciences, 370(1976), pp. 4748–4769. doi:10.1098/rsta.2011.0355.

[35] Wimperis, S. (1994) 'Broadband, narrowband, and passband composite pulses for use in advanced NMR experiments', Journal of Magnetic Resonance, Series A, 109(2), pp. 221–231.

doi:10.1006/jmra.1994.1159.

[36] Szwer, D.J. et al. (2010) 'Keeping a single qubit alive by experimental dynamic decoupling', Journal of Physics B: Atomic, Molecular and Optical Physics, 44(2), p. 025501. doi:10.1088/0953-4075/44/2/025501.

[37] Ali Ahmed, M.A., Álvarez, G.A. and Suter, D. (2013) 'Robustness of dynamical decoupling sequences', Physical Review A, 87(4). doi:10.1103/physreva.87.042309.

[38] Jones, J.A. (2013) 'Designing short robust NOT gates for quantum computation', Physical Review A, 87(5). doi:10.1103/physreva.87.052317.

[39] Souza, A.M., Álvarez, G.A. and Suter, D. (2012) 'Effects of time-reversal symmetry in dynamical decoupling', Physical Review A, 85(3). doi:10.1103/physreva.85.032306.

[40] QIC lecture notes 2024, C.S Adams, https://github.com/etotheipiequals/etotheipiequals/QIC$_{Latex}$

14. GENERAL SUMMARY

This report summaries ultracold molecules in electric and magnetic fields and shows some of their applications for quantum information. The different approximations commonly used are tested to find when they can be used. It shows how using microwave pulses can increase the time for experimental results to be stored without environmental noise impacting it. The effects of the type of pulses and the time the pulses are applied are consider and some basic simulations are shown of the different pulses used. Methods for deriving new pulses that work better under the most common experimental errors are shown and tested to show how future experiments can be improved. The concepts of the improved pulses are paired with the different pulse timings to show how the best pulse sequences can be found for a given experiment and show a large improvement in the lenght of time the environmental noise can be removed. Future concepts for pulse designs are mentioned to show how these results could be changed and improved if more time was available. All of these techniques combined should allow ultracold molecule experiments to reduce the effect of experimental errors in the future.

15. APPENDIX

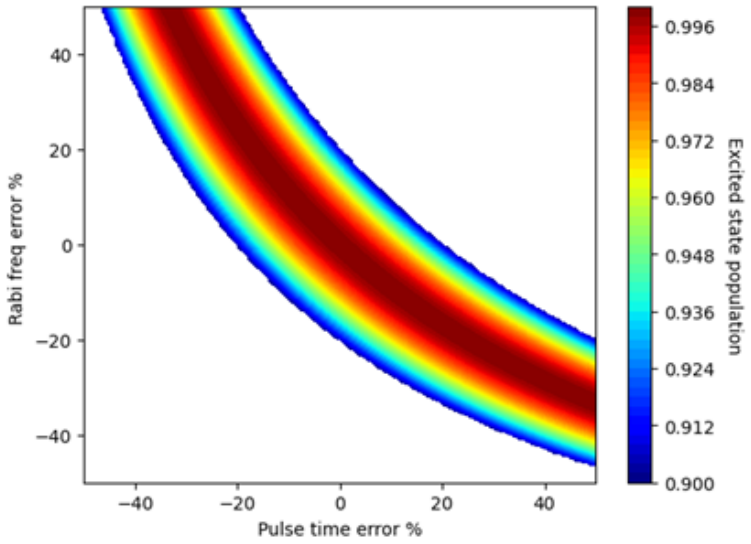

FIG. 21: By varying the Rabi frequency and the time of the pulse then measuring the final state, the relation between time and rabi frequency can be found. The 1/x shape of the curve shows they are inversely proportional.

$$U_{knill}\begin{pmatrix}1\\1\end{pmatrix}=\begin{pmatrix}1\\-1\end{pmatrix} \tag{33}$$

Applying the Knill pulse causes a phase of π up to a detuning of approximately half the Rabi frequency but applying an even number of Knill pulses cancels this phase so an even number has to be replaced in a decoupling sequence. When the detuning is too large, the effective Rabi frequency causes the effective pulse time to be much smaller and pulse flip angle errors start to accumulate.
where c = cos, s = sine

$$U_{XY}=\begin{pmatrix}C^2(B)+iS^2(B) & -iC(B)S(B)-S(B)C(B)\\ S(B)C(B)-iS(B)C(B) & -iS^2(B)+C^2(B)\end{pmatrix}, B=\Omega_{eff}t/2 \tag{34}$$

$$U_{XY4}=\begin{pmatrix}C^4(B)+2S^2C^2(B)-S^4-2iS^2C^2(B) & -2iC^3(B)S(B)-S(B)C^3(B)\\ -2iC^3(B)S(B)+S(B)C^3(B) & C^4(B)+2S^2C^2(B)-S^4-2iS^2C^2(B)\end{pmatrix} \tag{35}$$

C is Cosine, S is Sine. $U_{XY4}=U_{XY}U_{XY}$ Terms from flip errors cancel and when evaluated around B = π/2 it is much closer to the identity matrix for a larger pulse error.

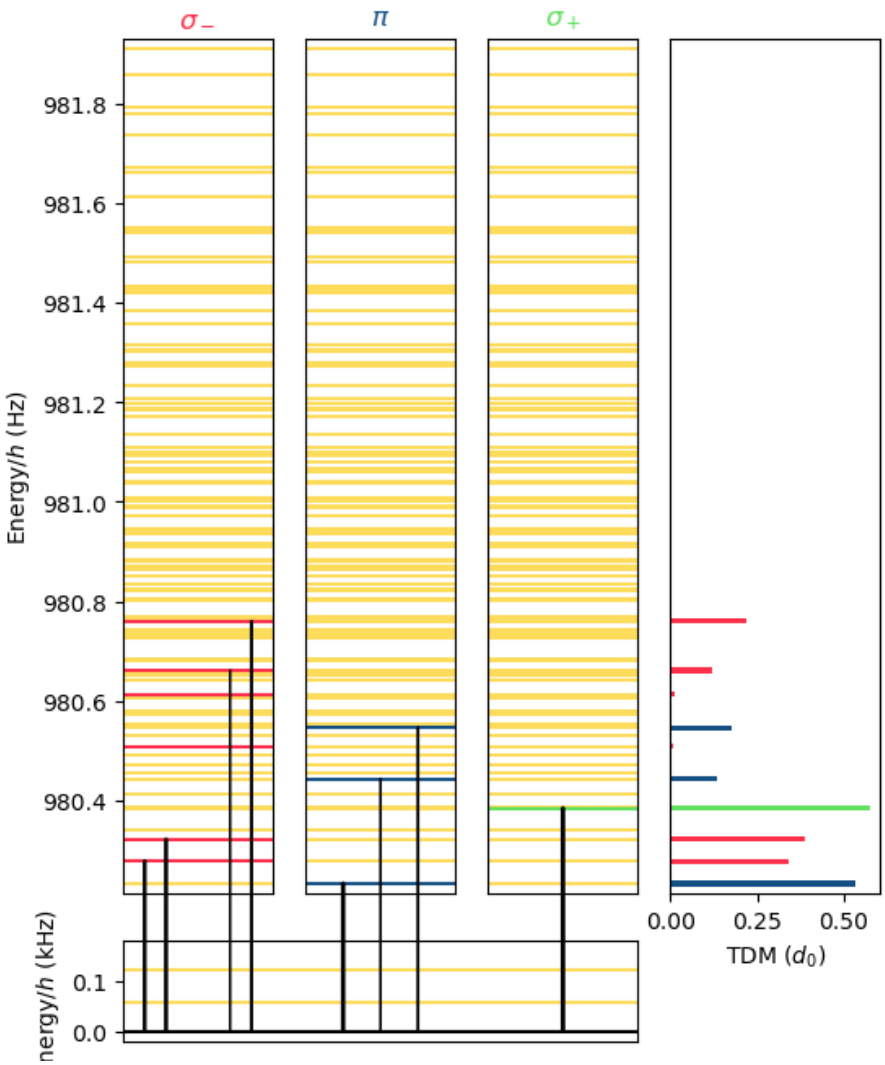

FIG. 22: Allowed transitions of RbCs from it's absolute ground state - spin stretch state.